AGU PUBLICATIONS

Geophysical Research Letters

RESEARCH LETTER
10.1002/2017GL072792

Key Points:
- The latest version of WACCM produces temperature trends in the Antarctic lower stratosphere in excellent agreement with past radiosondes
- The maximum trend is a third smaller than the largest trend in the previous version of WACCM
- The trend is due to a stronger Brewer-Dobson circulation and a warmer polar cap as a result of an updated parameterization of orographic gravity waves

Correspondence to:
N. Calvo,
nataliac@fis.ucm.es

Citation:
Calvo, N., R. R. Garcia, and D. E. Kinnison (2017), Revisiting Southern Hemisphere polar stratospheric temperature trends in WACCM: The role of dynamical forcing, *Geophys. Res. Lett.*, *44*, 3402–3410, doi:10.1002/2017GL072792.

Received 24 JAN 2017
Accepted 27 FEB 2017
Accepted article online 28 FEB 2017
Published online 15 APR 2017

Revisiting Southern Hemisphere polar stratospheric temperature trends in WACCM: The role of dynamical forcing

N. Calvo[1,2], R. R. Garcia[2], and D. E. Kinnison[2]

[1]Departamento de Física de la Tierra II, Facultad de Ciencias Físicas, Universidad Complutense de Madrid, Madrid, Spain, [2]Atmospheric Chemistry Observations and Modeling Laboratory, National Center for Atmospheric Research, Boulder, Colorado, USA

Abstract The latest version of the Whole Atmosphere Community Climate Model (WACCM), which includes a new chemistry scheme and an updated parameterization of orographic gravity waves, produces temperature trends in the Antarctic lower stratosphere in excellent agreement with radiosonde observations for 1969–1998 as regards magnitude, location, timing, and persistence. The maximum trend, reached in November at 100 hPa, is -4.4 ± 2.8 K decade^{-1}, which is a third smaller than the largest trend in the previous version of WACCM. Comparison with a simulation without the updated orographic gravity wave parameterization, together with analysis of the model's thermodynamic budget, reveals that the reduced trend is due to the effects of a stronger Brewer-Dobson circulation in the new simulations, which warms the polar cap. The effects are both direct (a trend in adiabatic warming in late spring) and indirect (a smaller trend in ozone, hence a smaller reduction in shortwave heating, due to the warmer environment).

1. Introduction

In the polar lower stratosphere of the Southern Hemisphere (SH), observations show a long-term cooling in the last decades of the twentieth century [*Thompson and Solomon*, 2002, 2005; *Randel et al*., 2009], which has been reproduced in general circulation models [e.g., *Gillet and Thompson* 2003]. Idealized simulations have attributed most of the trend in austral spring to ozone depletion [e.g., *McLandress et al*., 2011; *Polvani et al*., 2011]. The decrease in ozone leads to cooling, which enhances the meridional gradient of temperature in the SH polar cap and intensifies the zonal-mean zonal winds in the stratosphere and eventually also in the troposphere. In fact, simulations indicate that the long-term cooling leads to a poleward shift and strengthening of the tropospheric jet in austral summer [e.g., *Swart and Fyfe*, 2012; *Lee and Feldstein*, 2013], with impacts on the variability of storm tracks [*Yin*, 2005; *Grise et al*., 2014], precipitation [*Fyfe et al*., 2012; *Previdi and Polvani*, 2014], and the strength of the ocean circulation [*Russell et al*., 2006; *Bitz and Polvani*, 2012]. Therefore, accurate modeling of past ozone and temperature changes in the SH polar lower stratosphere is key for understanding their impacts on present SH climate and for predicting future changes.

The Chemistry-Climate Model Validation project (CCMVal-2) [*Stratospheric Processes and their Role in Climate Chemistry (SPARC) CCMVal*, 2010] evaluated the simulation of temperature trends in chemistry-climate models and concluded that the ensemble mean temperature trend in the SH polar cap was too large over 1969–1998 compared with observations by *Thompson and Solomon* [2002]. More recently, *Young et al*. [2013] compared several data sets of radiosonde and satellite observations, including those analyzed by *Thompson and Solomon* [2002] against ensemble mean trends from CCMVal-2 models and also from models that participated in CMIP5 (Coupled Model Inter-comparison Project, phase 5); they concluded that the ensemble mean trends in the lower stratosphere SH polar cap derived from either ensemble were not statistically different from observations, although there was large intermodel variability.

For the Whole Atmosphere Community Climate Model (WACCM), *Calvo et al*. [2012] reported a maximum polar cap (65–90°S) average trend of -6.2 ± 2.5 K decade^{-1} in the lower stratosphere in November for the period 1969–1998 in an ensemble of simulations that were part of CMIP5. This trend was about 30% larger than the November trends for the same period and region estimated from radiosonde observations by *Young et al.* [2013]. An even larger trend, -6.7 ± 3.0 K decade^{-1}, was obtained for the month of December, inconsistent with the radiosonde data, for which the largest trend occurs in November. Nevertheless, *Calvo*

et al. [2012] concluded that the temperature trend in WACCM-CMIP5 was not statistically different from the observations at the 95% confidence level. (These and all other trends in this study are quoted with 2σ uncertainty ranges.)

Although temperature changes in the Antarctic lower stratosphere respond mainly to ozone changes, they can also be modulated by changes in dynamics. Thus, an intensification of the mean meridional downwelling over Antarctica could partly offset the decrease in shortwave heating due to ozone loss, reducing the cooling trend. *Calvo et al*. [2012] found no significant trend in the modeled polar downwelling in the months when the largest temperature trends occur, and similar behavior was reported in most of the CCMVal-2 models [*Wang and Waugh*, 2012]. However, a stronger meridional circulation could also affect Antarctic temperature trends by producing a climatologically warmer background state, since heterogeneous ozone loss is slower under warmer conditions, and slower ozone loss moderates the decrease of shortwave heating.

The mean meridional circulation is driven by dissipation of planetary waves, which are resolved in WACCM, and gravity waves (GW), which are parameterized. The latest version of WACCM, which is being used for simulations in support of the Chemistry-Climate Model Initiative (CCMI), includes an updated parameterization of orographic GW, together with a new stratospheric chemistry scheme. *Garcia et al*. [2017] show that these improvements lead to a better representation of the dynamical and chemical structure of the Antarctic polar vortex without degrading the performance of the model in the Northern Hemisphere (NH). The present study revisits the question of temperature trends in the SH polar cap in the latest version of WACCM, comparing them with previous model simulations and observations. We show that the simulated temperature trends are now in excellent agreement with observations due to the effects of enhanced downwelling over Antarctica.

2. Model and Simulations

WACCM is the high-top atmospheric component of Community Earth System Model (CESM). It is a fully interactive chemistry-climate model with an upper boundary at about 140 km. The version of the model used here, version 4, has been updated in preparation for the CCMI intercomparison; we refer to this model as WACCM-CCMI. It differs from the WACCM version used for CMIP5, WACCM-CMIP5 [*Marsh et al*., 2013], in that it incorporates a new stratospheric chemistry scheme with a more realistic representation of heterogeneous chemistry, and a modified orographic GW parameterization. The modifications of the orographic GW parameterization have the effects of increasing the orographic source flux preferentially in the SH and thus affect most strongly the forcing of the Brewer-Dobson circulation (BDC) over the southern polar cap. Changes to the chemistry mechanism and the orographic GW parameterization, and the resulting improvements in the model climatology, are discussed in detail by *Garcia et al*. [2017]. They show that the modification of the gravity wave parameterization leads to a weaker Antarctic polar vortex and a stronger downwelling branch of the Brewer-Dobson circulation (BDC) over the austral polar cap, which warms the Antarctic polar stratosphere, reduces the cold pole bias present in previous versions of WACCM, and produces ozone vertical profiles and ozone column amounts that are in very good agreement with observations during Antarctic spring. At the same time, other desirable features of the model's climatology (NH winds and temperature, frequency and seasonal distribution of sudden stratospheric warming, and seasonal behavior of the polar mesopause) are preserved.

Here we analyze an ensemble of three simulations made with WACCM-CCMI using observed daily sea surface temperatures (SST), observed greenhouse gases and halogen concentrations at the surface, and observed sulfate heating from volcanic aerosols. The quasi-biennial oscillation is simulated by relaxing the equatorial zonal-mean zonal winds to observations. Solar spectral irradiance is prescribed from the model of *Lean et al*. [2005]. We refer to this ensemble of WACCM-CCMI simulations as REF-ORO. To understand the role that the new chemistry scheme and the new parameterization of orographic gravity waves play in the trends discussed here, one additional simulation is analyzed, similar to REF-ORO but without any changes to the orographic gravity wave parameterization; we refer to this simulation as REF. The only difference between REF and REF-ORO is the new parameterization of orographic gravity waves included in the latter. The simulations analyzed here are the same as those examined in *Garcia et al.* [2017].

Although the REF-ORO simulations are run with specified, observed SST, the trends in WACCM-CCMI simulations coupled to an ocean model are very similar (not shown), consistent with the results of *Sigmond et al.*

[2010], who found that atmosphere-ocean coupling plays a negligible role in the response to ozone depletion in the Canadian Middle Atmosphere Model. We analyze the REF-ORO simulations to make a clean comparison with the REF simulation, which was also run with prescribed sea surface temperatures.

3. Results

Figure 1a shows the seasonal cycle of SH polar cap (65–90°S) temperature trends as a function of pressure in the ensemble mean of the REF-ORO simulations. This and all other trends presented here are computed for the period 1969–1998, the same as considered by *Thompson and Solomon* [2002] and *Calvo et al.* [2012]. This period encompasses the inception and growth of the Antarctic ozone hole; after the late 1990s ozone loss stabilizes and temperature trends decrease, as noted by *Young et al*. [2013]. In addition, Antarctic temperature observations are available from several radiosonde data sets throughout the period [*Young et al*., 2013]. Linear trends and their significance were computed as in *Calvo et al*. [2012]: Monthly mean time series were averaged over the polar cap (65–90°S; weighted by the cosine of latitude) and then linear least squares fits were determined. Trends are considered significant at the 95% confidence level whenever they are larger than 2σ, where σ is the standard deviation of the trend corrected by the autocorrelation of the residuals of the linear fit [see, e.g., *Wilks*, 2006, chap. 6].

As seen in Figure 1a, the REF-ORO ensemble shows significant cooling from October to February in the middle and lower stratosphere. The trend peaks in November at 100 hPa, reaching -4.4 ± 2.8 K decade^{-1}. The spatial structure of the trend resembles that of the CMIP5 ensemble described by *Calvo et al*. [2012, Figure 1]. However, there are several important differences. First, the largest trend is reduced by about 34%, from -6.7 K decade^{-1} in WACCM-CMIP5 to -4.4 K decade^{-1} in REF-ORO (see Table 1). It also peaks earlier and at lower altitude (November at 100 hPa versus December at 80 hPa). Finally, the significant trend in the lower stratosphere does not extend as long into austral fall in REF-ORO as in CMIP5 (March versus April–May). The magnitude, location, and timing of the largest modeled trend are now in much better agreement with the radiosonde observations discussed by *Young et al*. [2013].

As noted earlier, ozone changes are the main contributor to temperature trends in the lower stratosphere in austral spring. Figure 1c shows the trend in zonal mean ozone as a function of month and pressure. As expected, the spatial pattern of the trend is similar to that of temperature, but the largest ozone trends precede the largest temperature trends. The maximum trend in ozone, -0.68 ± 0.32 ppmv decade^{-1}, occurs in October at 60 hPa. Compared to WACCM-CMIP5, the maximum ozone trend is reduced in REF-ORO by 20% and occurs at a lower level (60 hPa versus 40–50 hPa in WACCM-CMIP5; see Table 1). In addition, the persistence of the lower stratospheric ozone trend into austral fall is shortened in the new simulations.

To isolate the role that the parameterization of orographic GW plays in the reduction of the temperature trends, Figures 1b and 1d show the seasonal evolution of zonal mean temperature and ozone trends, respectively, as functions of pressure for the REF simulation, in which the new chemistry scheme is included but the new parameterization of orographic gravity is omitted. Without the additional forcing by orographic GW, temperature and ozone trends are larger than in REF-ORO; in November, temperature and ozone trends in the REF simulation reach -7.3 ± 4.2 K decade^{-1} and -0.84 ± 0.34 ppmv decade^{-1}, respectively. Moreover, the temperature trend is even larger in December, reaching -8.2 ± 4.0 K decade^{-1}. Interestingly, the behavior of the trends in WACCM-CCMI, simulation REF, is similar to that found in WACCM-CMIP5, which shares the same GW parameterization [cf. *Calvo et al*., 2012] (Table 1). In addition to the different magnitude, the largest trend occurs at higher altitude in REF than in REF-ORO, and significant trends extend longer into late austral fall. All of this suggests that the key difference between REF-ORO, on one hand, and REF and CMIP5, on the other, is the impact of enhanced GW forcing in REF-ORO, which produces a stronger meridional circulation.

To explore the influence of the BDC on temperature trends, we analyze the behavior of the processes that control the temperature budget in the Antarctic lower stratosphere. The thermodynamic equation in the transformed Eulerian mean (TEM) formulation can be written as

$$\frac{\partial \overline{T}}{\partial t} = -\overline{w}^* S + \overline{Q}_S + \overline{Q}_L \tag{1}$$

where $\overline{T}$ is the zonal mean temperature, $\overline{w}^*$ is the TEM vertical velocity, S is the atmospheric stability

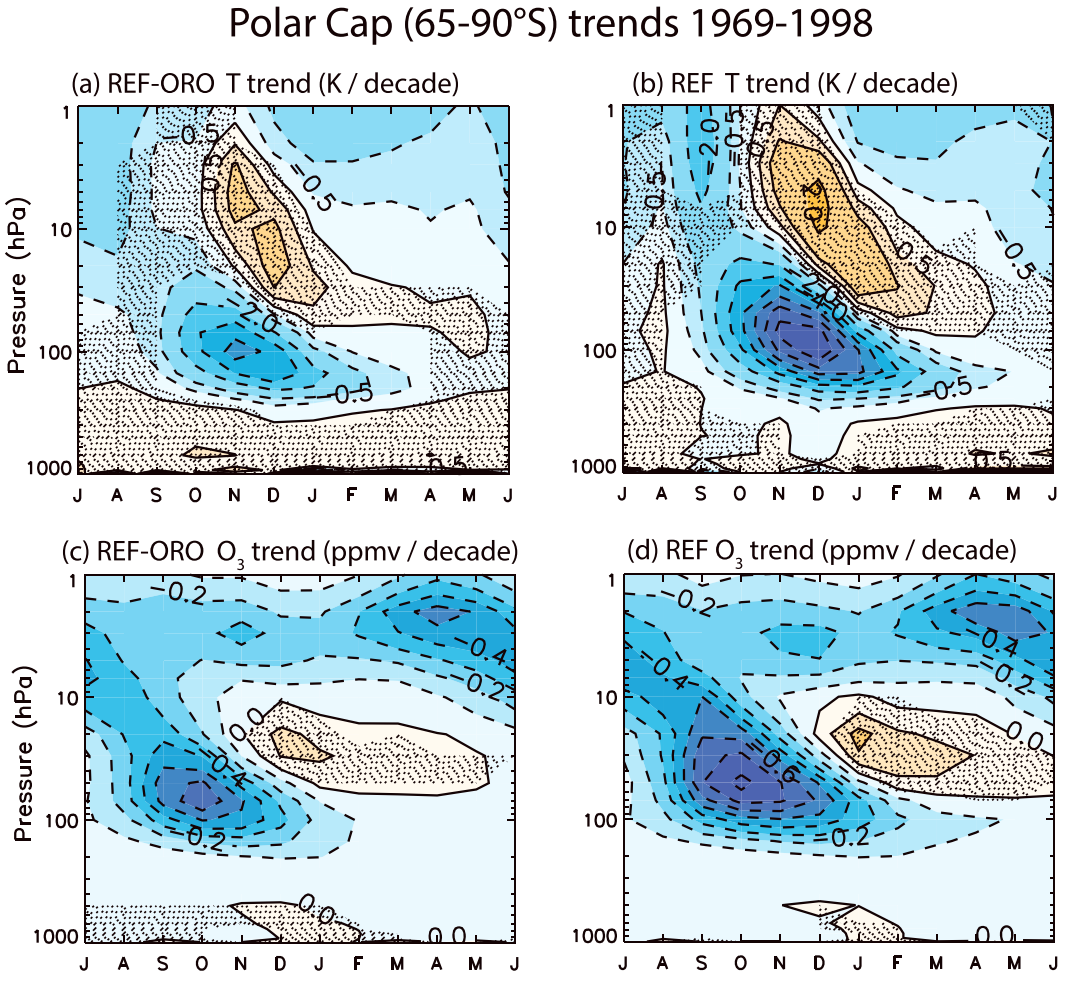

Figure 1. Ensemble mean trends for 1969–1998 of zonal mean temperature and ozone mixing ratio averaged over the polar cap (65–90°S) for simulations (a, c) REF-ORO and (b, d) REF. Units are K decade^{-1} and ppmv decade^{-1}. Contours are drawn every 0.5, 1, 2, K decade^{-1} and every 0.1 ppmv decade^{-1}. Shading denotes results not significant at the 95% confidence level.

parameter, and $\overline{Q}_S$ and $\overline{Q}_L$ are the zonal mean shortwave and longwave heating rates, respectively. In the region of interest, horizontal advection of temperature and GW diffusion are negligible and are disregarded here. Using equation (1), we may express the long-term trends in the various quantities as

$$\delta\left(\frac{\partial \overline{T}}{\partial t}\right) = \left[-\delta(\overline{w}^* S) + \delta\overline{Q}_S + \delta\overline{Q}_L\right] \tag{2}$$

where δ denotes the long-term trend. Assuming that the longwave heating rate, $\overline{Q}_L$, can be expressed as Newtonian cooling with relaxation rate α, equation (2) may be rewritten as

Table 1. Maximum Calculated and Observed Decadal Trends in Polar Cap (65–90°S) Zonal Mean Temperature and Ozone for 1969–1998[a]

	T Trend (K/Decade)	O_3 Trend (ppmv/Decade)	O_3 Column Trend (DU/Decade)
WACCM-CMIP5	−6.7 ± 3.0 (80 hPa; Dec)	−0.85 ± 0.32 (40–50 hPa; Oct)	
WACCM-CCMI (REF)	−8.2 ± 4.0 (100 hPa; Dec)	−0.84 ± 0.34 (50 hPa; Oct)	−58.5 ± 7.5
WACCM-CCMI (REF-ORO)	−4.4 ± 2.8 (100 hPa; Nov)	−0.68 ± 0.32 (60 hPa; Oct)	−47.5 ± 7.7
Radiosonde *T*, O_3 [*Young et al.*, 2013]	IUK: −4.7 ± 2.8; RICH-obs: −4.1 ± 2.4; HadAT2: −3.8 ± 2.4 (100 hPa; all in Nov)		−46
SPARC AC&C O_3 [*Cionni et al.*, 2011]		−0.89 ± 0.13 (50 hPa; Oct)	

[a]The level and month of the largest trend is indicated in each case together with its 2σ uncertainty range. The trends in the third column refer to the September–December mean ozone column. See text for details.

$$\delta\overline{T} = \frac{1}{\alpha}\left[-\delta(\overline{w}^* S) + \delta\overline{Q}_S - \delta\left(\frac{\partial\overline{T}}{\partial t}\right)\right] \quad (3)$$

which relates the long-term trend in temperature to the trends in adiabatic cooling or warming, shortwave heating rate, and time rate of change of temperature. The last of these must vanish in the annual mean but can contribute to monthly trends, in which case it may be interpreted as a change in the seasonal cycle of temperature.

The seasonal evolution as a function of altitude of the first two terms in brackets on the right-hand side (RHS) of equation (3) is shown in Figures 2a and 2c for the REF-ORO ensemble mean and in Figures 2b and 2d and the REF simulation. The results are shown in units of K decade^{-1}, as obtained after dividing each term by the thermal relaxation rate, α. For the latter we adopted a vertical profile based upon *Wehrbein and Leovy's* [1982] "25 km boxcar" Newtonian cooling coefficient, with values of 0.03 day^{-1} below 100 hPa, 0.1 day^{-1} at 20 hPa, and 0.2 day^{-1} at 1 hPa. The sum of all three terms on the RHS of equation (3) gives an estimate of the total temperature trend and is shown in Figures 2e and 2f. Comparison of Figures 2e and 2f with the actual temperature trends (Figures 1a and 1b) indicates reasonably close agreement, lending confidence to the methodology and assumptions adopted here. The last term on the RHS of equation (3), the trend in the time rate of change of temperature, is not negligible during the months surrounding the peak cooling. We have omitted it from Figure 2 in the interests of brevity, and because it represents part of the response to the processes (adiabatic cooling and warming, and shortwave heating) that actually drive the total temperature trend.

The trend in adiabatic cooling and warming is shown in Figures 2a and 2b. Below 10 hPa, it is small in simulation REF from September to November, becoming large and positive only in December, and especially in January, corresponding to the transition to summer in that simulation. This transition is accompanied by an abrupt acceleration of the BDC and a large trend in adiabatic warming. This is consistent with the findings of *Calvo et al.* [2012], who found little contribution by adiabatic processes to the temperature trend in WACCM-CMIP5 in the months when that trend is largest. In contrast, in REF-ORO the adiabatic term is important already in November, when it contributes 1 to 1.5 K decade^{-1} to the total temperature trend; it remains substantial throughout the transition to summer but without the abrupt change seen in simulation REF in January. The different behavior of these trends follows from the different seasonal evolution of the polar vortex in the two simulations. As discussed by *Garcia et al.*, [2017], the weak BDC in the REF simulation allows extreme cooling of the Antarctic polar cap during winter and spring, leading to an unrealistically strong polar vortex in the lower stratosphere and a transition to summer conditions that is delayed by more than a month compared to observations.

The impact of the BDC on temperature trends is not limited to the behavior in late austral spring, even though important trends in adiabatic warming are present mainly during that season. Figures 2c and 2d show large differences in the contribution of shortwave heating to the temperature trend beginning in September, when sunlight returns to Antarctica, and lasting throughout the transition to summer. The largest contribution is about -5 K decade^{-1} in the REF-ORO ensemble compared to over -6 K decade^{-1} in the REF simulation. These contributions are commensurate with the maximum ozone trends shown in Figure 1 and Table 1 (-0.68 and -0.84 ppmv decade^{-1}, respectively), and they are ultimately explained by the impact of mean meridional downwelling on temperature, and of temperature on ozone destruction, as illustrated next.

Figure 3 compares the evolution of the chemical lifetime of ozone over Antarctica in September during 1969–1998. The lifetime, τ, was estimated from model results by dividing the loss rate of ozone (ppmv d^{-1}) by its mixing ratio (ppmv) [see, e.g., *Brasseur and Solomon*, 1986, chap. 5]. Figure 3 shows that τ is shorter everywhere in simulation REF than in REF-ORO (similar results, not shown, are obtained for October). This is a consequence of the strong sensitivity of heterogeneous ozone loss to stratospheric temperatures, which are substantially colder in REF than in REF-ORO throughout austral winter and spring. *Garcia et al.*, [2017, Figures 3 and 10] show that September and October time-mean temperatures in the lower stratosphere are about 5–6 K colder in REF than in REF-ORO; in winter (June–August), the season of formation of polar stratospheric clouds, they are 3–4 K colder, as a result of the stronger polar downwelling present in simulation REF-ORO. Colder temperatures promote the formation of polar stratospheric clouds and enhance ozone loss by heterogeneous chemical reactions. When $\tau \leq 50$ days, severe ozone loss can occur in the time span of Antarctic spring.

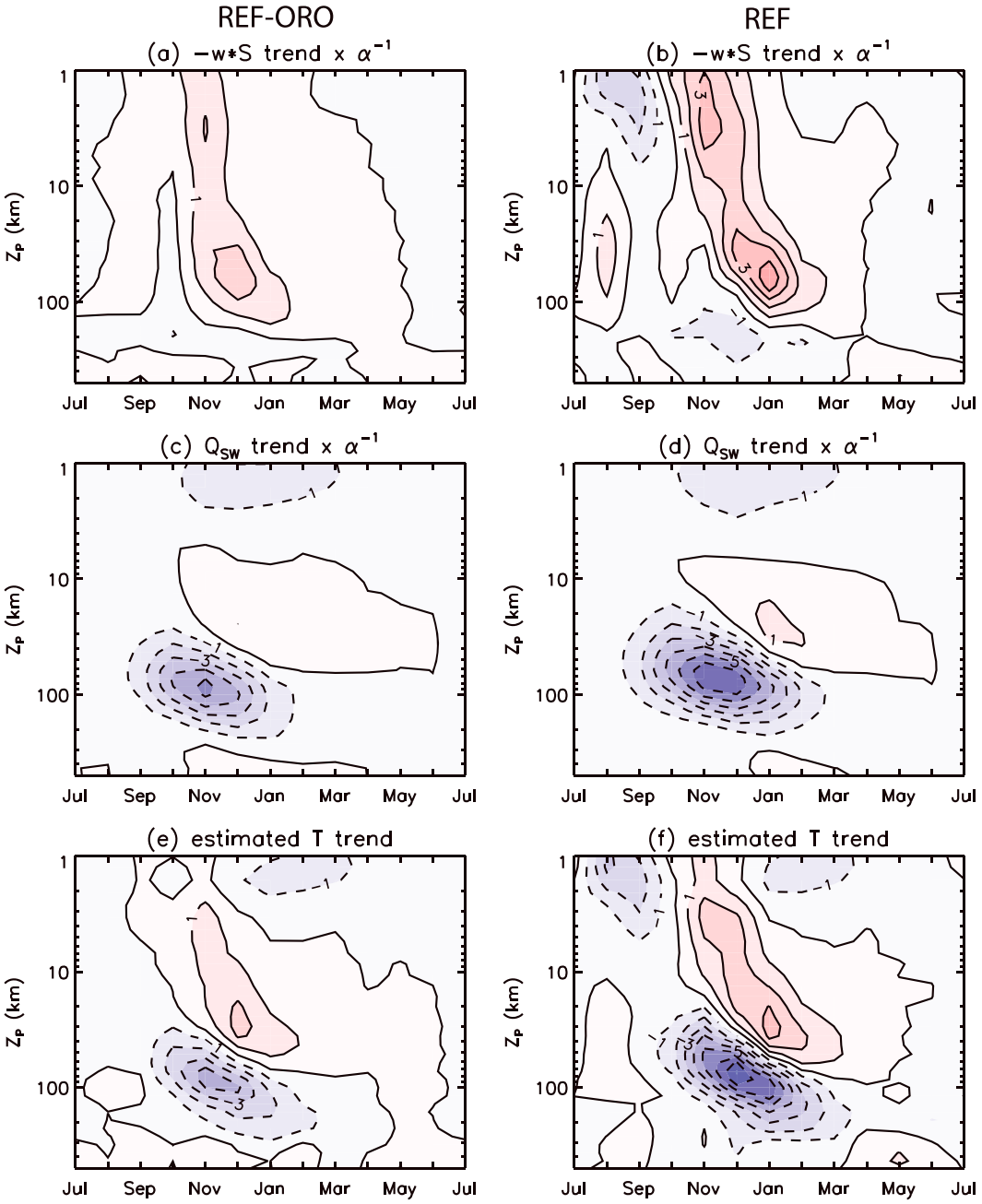

Figure 2. Contributions to temperature trends (K decade^{-1}) by individual terms in the TEM thermodynamic equation for simulations (a, c, and e) REF-ORO and (b, d, and f) REF. The contributions are estimated by dividing the trends in the thermodynamic equation by the local value of the infrared radiative relaxation rate. Figures 2a and 2b are the contributions due to trends in adiabatic cooling and warming, and Figures 2c and 2d are the contributions due to trends in shortwave heating. The total temperature trend obtained from the sum of all contributions on the RHS of equation (3) is shown in Figures 2e and 2f. The contour interval is 1 K decade^{-1}. See text for details.

As seen in Figure 3, τ drops below 50 days in simulation REF throughout the lower Antarctic stratosphere in the early 1980s, whereas this does not occur in REF-ORO until the 1990s, and then only below 40 hPa. Evidently, ozone-temperature feedbacks are less efficient in the warmer polar environment of simulation REF-ORO than in REF. As a consequence, ozone loss and ozone trends are smaller (and are confined to lower altitudes) in REF-ORO than in REF. The less severe ozone loss in simulation REF leads to smaller negative trends in shortwave heating and is ultimately responsible for the smaller temperature trends in simulation

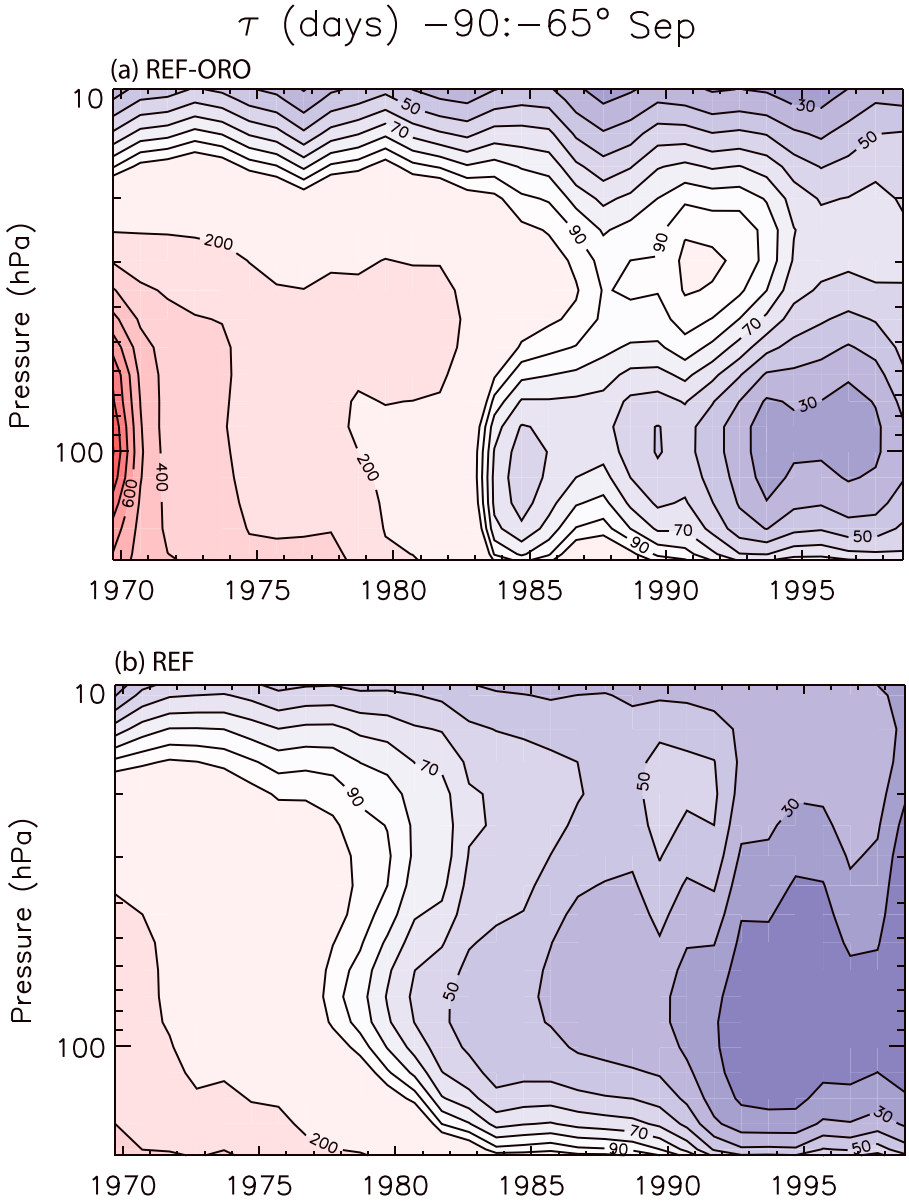

Figure 3. Photochemical lifetime (days) of ozone for simulations (a) REF-ORO and (b) REF as a function of time and altitude. Contour are shown every 10 days up to 100 days and every 100 days thereafter.

REF-ORO through November, when important trends in adiabatic warming come into play in REF-ORO, and through December in REF.

4. Summary and Discussion

We have shown that new simulations carried out with an updated version of WACCM (WACCM-CCMI) display temperature trends in the polar cap over Antarctica that are in excellent agreement with radiosonde temperature observations for the period 1969–1998. The largest temperature trend in the ensemble mean of these new simulations, denoted by REF-ORO, is -4.4 ± 2.8 K decade^{-1} and is reached in November at 100 hPa. *Young et al.* [2013] compared several radiosonde data sets and reported maximum cooling values of -4.7 ± 2.8 K decade^{-1} from the Iterative Universal Kriging (IUK) radiosonde analysis project, -4.1 ± 2.4 K decade^{-1} from the Radiosonde Innovation Composite Homogenization-obs, version 1.5 (RICH-obs), and -3.8 ± 2.4 K decade^{-1} for the Hadley Center Atmospheric Temperature data set, version 2

(HadAT2); thus, the largest cooling trend in WACCM-CCMI lies well within the range of the radiosonde values and occurs in the same month and at the same altitude as in the observations. The simulated trend represents a marked improvement compared to that computed with the previous version of WACCM, WACCM-CMIP5, which was -6.7 ± 3.0 K decade^{-1} and occurred at higher levels (80 hPa) and persisted longer, into November and December.

Two main changes are present in the new REF-ORO simulations compared to WACCM-CMIP5: A new heterogeneous chemistry scheme and a modified parameterization of orographic GW. As discussed by *Garcia et al.* [2017], the former improves the simulation of polar chemistry, while the latter forces stronger downwelling over Antarctica and reduces the model's cold pole bias. An additional simulation made with WACCM-CCMI, denoted here as REF and differing from REF-ORO only in the omission of changes in the gravity wave parameterization, produces polar temperature trends that resemble those in WACCM-CMIP5 as regards the magnitude and altitude of the maximum trends and their persistence. Thus, the smaller temperature trends in REF-ORO are evidently due to the stronger BDC. An analysis of long-term trends based upon the TEM thermodynamic budget indicates that enhanced adiabatic warming in REF-ORO moderates the temperature trend caused by the development of the ozone hole and reduces its persistence.

Although the REF-ORO simulations produce trends in Antarctic polar cap temperature that are much smaller than in previous versions of WACCM, and much more consistent with observations, they also produce maximum ozone trends that are ~20% lower. *Calvo et al.* [2012] discussed the ozone trend derived from the SPARC data set [*Cionni et al.*, 2011] for 1969–1998; that trend peaks at -0.89 ± 0.13 ppmv decade^{-1}, at 50 hPa in October. This agrees more closely with the trends obtained from the CMIP5 and REF simulations than with the trend from REF-ORO (see Table 1). However, the adequacy of the SPARC ozone trend for 1969–1998 is questionable. SPARC ozone is derived from the data set of *Randel and Wu* [2007], which in the southern polar cap below 30 hPa consists of radiosonde observations for the period 1979–2005 from a single location (Syowa; 69°S). The observations are fit with a linear regression on equivalent effective stratospheric chlorine and assigned to the southern polar cap (65–90°). Ozone data before 1979 can be obtained from the regression fit, but they do not represent actual observations, and the linear fit itself does not account for interannual dynamical variability.

On the other hand, total ozone observations are available for the entire period 1969–1998 from several Antarctic stations [*Young et al.*, 2013]. Young et al. calculated the trend of seasonal-mean (September–December) polar cap (65–90°S) total ozone and obtained a value of -46 Dobson unit (DU) decade^{-1} for the period 1969–1998 (see their Figure 4 and related discussion). In WACCM, a similar calculation yields trends of -47.5 ± 7.7 DU decade^{-1} for the REF-ORO ensemble and -58.5 ± 7.5 DU decade^{-1} for the REF simulation. Thus, as regards seasonal column ozone trends, the REF-ORO results are in excellent agreement with observations.

Overall, our results demonstrate that modifications to WACCM that reduce the cold pole bias also improve the representation of temperature trends in the lower stratosphere over Antarctica, making them much more consistent with available observations. These improvements will facilitate understanding past ozone-related climate change and result in more accurate forecasts of ozone and temperature changes in the future.

Acknowledgments
We thank W.J. Randel and two anonymous reviewers for their comments, which have resulted in an improved paper. The National Center for Atmospheric Research (NCAR) is sponsored by the U.S. National Science Foundation (NSF). N. Calvo acknowledges partial support from the European Project 603557-STRATOCLIM under program FP7-ENV.2013.6.1-2 and from the Spanish Ministry of Economy and Competitiveness through the PALEOSTRAT (CGL2015-69699-R) project. R.R. Garcia was supported in part by NASA grant X09AJ83G; and D.E. Kinnison was supported in part by NSF Frontiers in Earth System Dynamics grant OCE-1338814. WACCM is a component of NCAR's CESM, which is supported by the NSF and the Office of Science of the U.S. Department of Energy. Computing resources were provided by NCAR's Climate Simulation Laboratory, sponsored by NSF and other agencies. This research was enabled by the computational and storage resources of NCAR's Computational and Information Systems Laboratory (CISL). The ozone and temperature data used in this study are available from the references cited; model output has been stored at NCAR and is available from the authors.

References

Bitz, C. M. and L. M. Polvani (2012), Antarctic climate response to stratospheric ozone depletion in a fine resolution ocean climate model, *Geophys. Res. Lett.*, *39*, L20705, doi:10.1029/2012GL053393.

Brasseur, G., and S. Solomon (1986), *Aeronomy of the Middle Atmosphere*, pp. 452, D. Reidel, Dordrecht, Netherlands.

Calvo, N., R. R. Garcia, D. R. Marsh, M. J. Mills, D. E. Kinnison, and P. J. Young (2012), Reconciling modeled and observed temperature trends over Antarctica, *Geophys. Res. Lett.*, *39*, L16803, doi:10.1029/2012GL052526.

Cionni, I., et al. (2011), Ozone database in support of CMIP5 simulations: Results and corresponding radiative forcing, *Atmos. Chem. Phys. Discuss.*, *11*, 10,875–10,933, doi:10.5194/acpd-11-10875-2011.

Fyfe, J. C., N. P. Gillet and G. J. Marshall (2012), Human influence on extratropical Southern Hemisphere summer precipitation, *Geophys. Res. Lett.*, *39*, L23711, doi:10.1029/2012GL054199.

Garcia, R. R., A. K. Smith, D. E. Kinnison, A. de la Cámara, and D. J. Murphy (2017), Modification of the gravity wave parameterization in the Whole Atmosphere Community Climate Model: Motivation and results, *J. Atmos. Sci.*, *74*, 275–291, doi:10.1175/JAS-D-16-0104.1.

Gillet, N. P., and D. W. J. Thompson (2003), Simulations of Recent Southern Hemisphere climate change, *Science*, *302*(5643), 273–275, doi:10.1026/science.1087440.

Grise, K. M., S.-W. Son, G. J. P. Correa and L. M. Polvani (2014), The response of extratropical cyclones in teh Southern Hemisphere to stratospheric ozone depletion in the 20th century, *Atmos. Sci. Lett.*, *15*, 29–36, doi:10.1002/asl2.458.

Lean, J., G. Rottman, J. Harder, and G. Kopp (2005), SORCE contributions to new understanding of global change and solar variability, *Sol. Phys.*, *230*, 27–53, doi:10.1007/s11207-005-1527-2.

Lee, S., and S. B. Feldstein (2013), Detecting ozone-and greenhouse gas-driven wind trends with observational data, *Science*, *339*, 563–567, doi:10.1126/science.1225154.

Marsh, D. R., M. J. Mills, D. E. Kinnison, J.-F. Lamarque, N. Calvo, and L. M. Polvani (2013), Climate change from 1850 to 2005 simulated in CESM1 [WACCM], *J. Clim.*, *26*, doi:10.1175/JCLI-D-12-00558.1.

McLandress, C., T. G. Shepherd, J. F. Scinocca, D. A. Plummer, M. Sigmond, A. I. Jonsson, and M. C. Reader (2011), Separating the dynamical effects of climate change and ozone depletion. Part II: Southern hemisphere troposphere, *J. Clim.*, *24*, doi:10.1175/2010JCLI3958.1.

Polvani, L. M., D. W. Waugh, G. J. P. Correa, and S. W. Son (2011), Stratospheric ozone depletion: The main driver of 20th century atmospheric circulation changes in the Southern Hemisphere, *J. Clim.*, *24*, 795–812, doi:10.1175/2010JCLI3772.1.

Previdi, M. and L. M. Polvani (2014), Climate System Response to Stratospheric Ozone depletion and recovery, *Q. J. R. Meteorol. Soc.*, *140*, 2401–2419, doi:10.1002/qj.2330.

Randel, W. J., and F. Wu (2007), A stratospheric ozone profile data set for 1979–2005: Variability, trends, and comparisons with column ozone data, *J. Geophys. Res.*, *112*, D06313, doi:10.1029/2006JD007339.

Randel, W. J., et al. (2009), An update of observed stratospheric temperature trends, *J. Geophys. Res.*, *114*, D02107, doi:10.1029/2008JD010421.

Russell, J. K., W. Dixon, A. Gnanadesikan, R. J. Stouffer, and J. R. Toggweiler (2006), The Southern Hemispherewesterlies in a warming world: Propping open the door to the deep ocean, *J. Clim.*, *19*, 6382–6390, doi:10.1029/2010GL043773.

Sigmond, M., J. C. Fyfe, and J. F. Scinocca (2010), Does the ocean impact the atmospheric response to stratospheric ozone depletion?, *Geophys. Res. Lett.*, *37*, L12706, doi:10.1029/2010GL043773.

Stratospheric Processes and their Role in Climate Chemistry-Climate Model Validation (2010), SPARC report on the evaluation of chemistry climate models, Edited by V. Eyring, T. G. Shepherd and D. W. Waugh, SPARC Report No. 5, WCRP-132, WMO/TD1526. [Available at http://www.sparc-climate.org/publications/sparc-reports/.]

Swart, N. C. and J. C. Fyfe (2012), Observed and simulated changes in the Southern Hemisphere surface westerly wind stress, *Geophys. Res. Lett.*, *39*, 16, doi:10.1029/2012GL052810.

Thompson, D. W. J., and S. Solomon (2002), Interpretation of recent Southern Hemisphere climate change, *Science*, *296*, 895–899.

Thompson, D. W. J., and S. Solomon (2005), Recent stratospheric climate trends as evidence in radiosonde data: Global structure and tropospheric linkages, *J. Clim.*, *18*, 4785–4795.

Wang, L., and D. W. Waugh (2012), Chemistry-climate model simulations of recent trends in lower stratospheric temperatures and stratospheric residual circulation, *J. Geophys. Res.*, *117*, D09109, doi:10.1029/2011JD017130.

Wehrbein, W. M., and C. B. Leovy (1982), An accurate heating and cooling algorithm for use in a dynamical model of the middle atmosphere, *J. Geophys. Res.*, *39*, 1532–1544, doi:10.1175/1520-0469(1982)039<1532:AARHAC>2.0.CO;2.

Wilks, D. S. (2006), *Statistical Methods in the Atmospheric Sciences*, pp. 627, Elsevier, Amsterdam.

Yin, J. H. (2005), A consistent poleward shift of the storm tracks in simulations of the 21st century climate, *Geophys. Res. Lett.*, *32*, L18701, doi:10.1029/2005GL023684.

Young, P. J., A. H. Butler, N. Calvo, L. Haimberger, P. J. Kushner, D. R. Marsh, W. J. Randel, and K. H. Rosenlof (2013), Agreement in late twentieth century Southern Hemisphere stratospheric temperature trends in observations and CCMVal-2, CMIP3 and CMIP5 models, *J. Geophys. Res. Atmos.*, *118*, 1–9, doi:10.1002/jgrd.50126.